



# Insight into the Dzyaloshinskii-Moriya interaction through first-principles study of chiral magnetic structures

L. M. Sandratskii

*Max-Planck-Institut für Mikrostrukturphysik, Weinberg 2, 06120 Halle, Germany*

(Received 9 May 2017; revised manuscript received 10 July 2017; published 31 July 2017)

The purpose of the paper is to gain deeper insight into microscopic formation of the Dzyaloshinskii-Moriya interaction (DMI). The paper aims at the development of the physical picture able to address apparently contradicting conclusions of recent studies concerning the location of the DMI energy in the real and reciprocal spaces as well as the relation between values of the atomic moments and the DMI strength. The main tools of our study are the first-principles calculations of the energies of the spiral magnetic states with opposite chiralities. We suggest a method of the calculation of the spiral structures with account for the spin-orbit coupling (SOC). It is based on the application of the generalized Bloch theorem and generalized Bloch functions and allows to reduce the consideration of arbitrary incommensurate spiral to small chemical unit cell. The method neglects the anisotropy in the plane orthogonal to the rotation axis of the spirals that does not influence importantly the DMI energy. For comparison, the supercell calculation with full account for the SOC is performed. The concrete calculations are performed for the Co/Pt bilayer. We consider the distribution of the DMI energy in both real and reciprocal spaces and the dependence of the DMI on the number of electrons. The results of the calculations reveal a number of energy compensations in the formation of the DMI. Thus, the partial atomic contributions as functions of the spiral wave vector  $\mathbf{q}$  are nonmonotonic and have strongly varying slopes. However, in the total DMI energy these atom-related features compensate each other, resulting in a smooth  $\mathbf{q}$  dependence. The reason for the peculiar form of the partial DMI contributions is a  $\mathbf{q}$ -dependent difference in the charge distribution between  $\mathbf{q}$  and  $-\mathbf{q}$  spirals. The strongly  $\mathbf{q}$ -dependent relation between atomic contributions shows that the real-space distribution of the DMI energy obtained for a selected  $\mathbf{q}$  value cannot be considered as a general characteristic of a given material. Our study shows that it is physically most consistent to consider the electronic hybridization as a primary effect reflecting the nature of the DMI whereas the  $\mathbf{q}$ -dependent real-space distribution of the DMI energy is a consequence of the complex processes in the electronic structure including the charge transfer process. The physical process of the DMI formation is connected with the difference in the hybridization of the Co and Pt states for  $\mathbf{q}$  and  $-\mathbf{q}$  spirals under the influence of the SOC and broken spatial inversion. It depends sensitively on details of the electronic structure. The calculations with constraints on the values of the Co and Pt atomic moments show that there is no direct relation between these atomic quantities and the DMI strength since the details of the electronic structure crucial for the DMI are not reflected in these integral characteristics. The application of the method to the calculation of the magnon energies in systems with DMI is briefly addressed.

DOI: [10.1103/PhysRevB.96.024450](https://doi.org/10.1103/PhysRevB.96.024450)

## I. INTRODUCTION

Chiral magnetic structures play an important role in the modern physics. The recent discoveries in this field are related to the physics of magnetic skyrmions [1–5], fast-moving chiral domain walls [6–8], topological Hall effect [9], and magnetoelectric effects [10,11]. Two types of the chiral magnetic structures that were discovered and understood first are weak ferromagnets (WFs) [12,13] and spiral structures of the relativistic origin, relativistic spirals (RSs) [14,15]. These two physical phenomena can be considered as providing the basis for the understanding of the formation of more complex chiral structures. The phenomenon of the weak ferromagnetism consists in the appearance of a small ferromagnetic component in the material expected to be a compensated antiferromagnet [Fig. 1(a)]. Rather similar, the spiral structure of the relativistic origin appears in the materials expected to be collinear magnets [Fig. 1(b)] and usually has a long wavelength. There are two important features inherent for both WF and relativistic spirals. First, the instability of the achiral collinear states with respect to the formation of the chiral noncollinear magnetic structures and, second, different energies of the magnetic structures with opposite magnetic

chiralities. The latter feature leads to the physical realization of the structure with only one of the chiralities.

A seminal contribution to the understanding of the preferred formation in nature of the magnetic states with certain chirality was made by Dzyaloshinskii [12]. He explained the origin of the WF in  $\text{Fe}_2\text{O}_3$  by the property that the canting of the magnetic moments from the collinear antiferromagnetic configuration does not change the symmetry of the system. Since the collinear antiferromagnetic state corresponding to angle  $\phi = 0$  [Fig. 1(a)] is not distinguished by symmetry with respect to the canted states with  $\phi \neq 0$ , the minimum of the total energy cannot be at  $\phi = 0$ . Indeed,  $\phi = 0$  is just one selected point from the continuum of equivalent points [16]. While there is no symmetry operation transforming the canted magnetic structure characterized by canting angle  $\phi$  to the structure characterized by angle  $-\phi$ , these two structures are inequivalent and have different energies. Therefore, the energy curve as a function of canting angle  $E(\phi)$  is not symmetric with respect to the change of the sign of  $\phi$  and the minimum happens at an “accidental” nonzero value of  $\phi$  leading to a nonzero ferromagnetic component (Fig. 2).

We emphasize that the necessary conditions for the asymmetry of the energy curve  $E(\phi)$  are the accounting for the

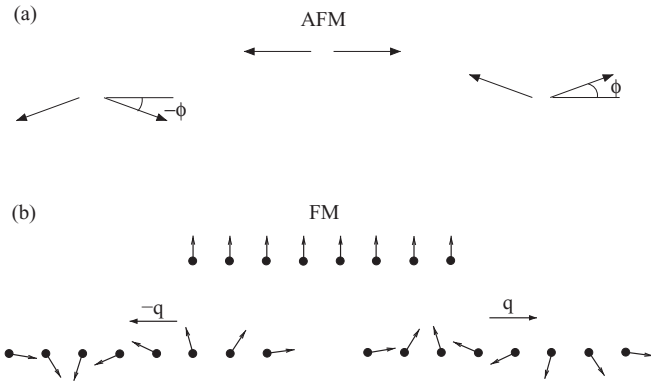


FIG. 1. (a) Schematic presentation of the achiral antiferromagnetic structure and two canted structures with opposite chiralities. (b) Schematic presentation of the achiral ferromagnetic structure and two spiral structures with opposite chiralities.

spin-orbit coupling (SOC) and the absence of the spatial inversion in the symmetry group of the atomic lattice [12,13]. The neglect of the SOC increases the symmetry of the system, leading to the equivalence of the states with opposite canting angles  $\phi$  and  $-\phi$ , and an extremum of  $E(\phi)$  at  $\phi = 0$  [16,17].

Similar arguments are valid in the case of relativistic spiral structures. If the SOC is neglected, the spirals with the vectors  $\mathbf{q}$  and  $-\mathbf{q}$  are equivalent, and symmetric curve  $E(\mathbf{q})$  has an extremum at  $\mathbf{q} = 0$  (Fig. 2). If the SOC is taken into account and the spatial inversion is not a symmetry operation of the atomic lattice,  $E(\mathbf{q}) \neq E(-\mathbf{q})$  and we deal again with an asymmetric curve of the type discussed above for the case

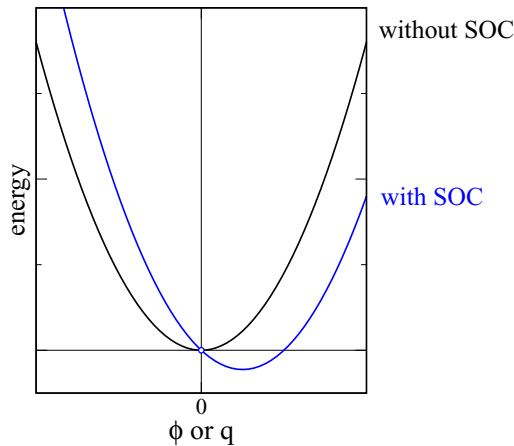


FIG. 2. Schematic presentation of the energy of the system as a function of the chirality parameter  $\xi$ .  $\xi = \phi$  in the case of WF and  $\xi = q$  in the case of RS. If the SOC is not taken into account, function  $E(\xi)$  is symmetric with respect to the sign reversal of  $\xi$ . If the SOC is taken into account, the symmetry decreases and the condition  $E(\xi) = E(-\xi)$  does not apply, leading to asymmetric energy curve with the minimum shifted to an accidental point. In the case of RS the curve  $E(q)$  is not continuous at  $q = 0$  that is indicated by the empty sphere on the energy curve. The actual value of the energy of the collinear state ( $q = 0$ ) is lower than the position of the sphere by the value dependent on the strength of the magnetic anisotropy.

of WF. (Some important differences between WF and RS will be addressed in Sec. II.)

If we aim to describe such an asymmetric energy curve within the model of interacting atomic moments, we notice that this description cannot be achieved in terms of the Heisenberg Hamiltonian

$$H_{\text{Heis}} = \frac{1}{N} \sum_{ij} J_{ij} \hat{\mathbf{S}}_i \cdot \hat{\mathbf{S}}_j \quad (1)$$

and needs additionally the energy term of the type

$$H_{\text{DMI}} = \frac{1}{N} \sum_{ij} \mathbf{D}_{ij} \cdot [\hat{\mathbf{S}}_i \times \hat{\mathbf{S}}_j], \quad (2)$$

commonly referred to as Dzyaloshinskii-Moriya interaction (DMI). Here,  $i, j$  number the magnetic atoms,  $\hat{\mathbf{S}}_i$  is the unit vector in the direction of the  $i$ th atomic moment,  $J_{ij}$  are interatomic Heisenberg exchange parameters,  $\mathbf{D}_{ij}$  are vector parameters of the interatomic DMI, and  $N$  is the number of magnetic atoms. The vector products of the atomic moments are different for the magnetic structures with opposite chiralities, whereas the scalar products entering the Heisenberg Hamiltonian do not depend on the sign of parameters  $\phi$  and  $\mathbf{q}$  defining the chirality of the magnetic structure (Fig. 1).

The expression (2) for the DMI energy has been intensively used in the model Hamiltonian studies of the systems with chiral magnetic order. Therefore, the evaluation of the parameters  $\mathbf{D}$  has become an important task for the first-principles calculations. There are many approaches suggested for the calculation of the DMI parameters. References [18–22] deal with the analytical derivatives of the total energy with respect to the infinitesimal deviations of the atomic moments from the collinear structure, Heide *et al.* [23] consider first-order perturbation theory for the electronic states of the nonrelativistic spiral structures, Freimuth *et al.* [25] suggest the expressions based on the Berry-phase approach, Yang *et al.* [26] employ supercell calculations for spiral structures, Koretsune *et al.* [27] consider the derivative of the spin-correlation function with respect to the wave vector, and Kikuchi *et al.* [28] suggest the expression for the DMI parameters in terms of spin current.

Mathematically, the first-principles approaches suggested for the calculation of the DMI energy are rather different. On the other hand, the physical basis of the DMI is common for all approaches and consists of the spin polarization of the electronic states, low symmetry of the atomic lattice, accounting for SOC. Therefore, the fact that different recent studies have arrived at apparently contradicting conclusions about important aspects of the physics of the DMI demands for careful analysis. A remarkable example of such apparently contradicting conclusions is provided by the recent studies of the Co/Pt bilayers. Thus, Yang *et al.* [26] in their theoretical work have come to the conclusion that the energy of the DMI interaction between Co spins is predominantly located at the Pt atoms. They make a remark on the presence of frequent confusion in the recent publications concerning the relation between spatial location of the interacting spin moments and of the energy of the interaction. On the other hand, the statement by Yang *et al.* of the predominant real-space location of the DMI energy on the Pt atoms seems to disagree with the conclusions of several other studies, arguing that the main

contribution to the DMI energy comes from the points in the *reciprocal* space where the so-called avoided crossing of the electronic bands takes place [27,28]. According to this viewpoint, not the real-space distribution of the DMI energy but the properties of the electronic states in the reciprocal space must be in the focus of the consideration.

Another important conclusion of Yang *et al.* [26] concerning the microscopic nature of the DMI is the absence of the direct correlation between induced Pt moment and the DMI strength that challenges the opposite conclusion of Ryu *et al.* [29] arguing to establish a close relation between these two quantities.

Our purpose in this paper is to gain deeper insight into the microscopic formation of the DMI energy. In particular, we investigate in detail the location of the DMI energy in the real and reciprocal spaces aiming to address the apparent discrepancies between the conclusions of previous studies.

We apply two different calculation methods to investigate the chiral spiral structures. One of the applied methods is suggested in this paper. It is based on the use of the generalized Bloch functions [17,30] and has features common with the approach by Heide *et al.* [23,31] but not equivalent to it and has important new properties. The second method is a straightforward supercell approach. Here, the size of the supercell is determined by the periodicity of the considered spiral structure. This feature limits the practical feasibility of the method to the commensurate spiral structures with reasonably small wavelengths commensurate with the lattice. On the other hand, the supercell method is free of the approximations of the first method and can be used for its testing. The supercell approach was employed in the work by Yang *et al.* [26]. As the concrete object of study we have chosen the prototype thin-film DMI system of the Co/Pt bilayer.

The paper is organized as follows. In Sec. II we briefly discuss the difference of the WF and RS from the viewpoint of the first-principles calculations and introduce DMI energy as the difference of the energies of the RS with opposite chirality. In Sec. III we introduce a method for the first-principles calculation of the RS. Section IV contains the results of the calculations and their discussion. Section V provides the conclusions.

## II. GENERAL REMARKS

Above, we pointed out common features of the  $E(\xi)$  for both WF and RS, where  $\xi$  is either  $\phi$  or  $\mathbf{q}$ . It is instructive to discuss here the difference of the two physical phenomena from the viewpoint of the first-principles calculations. In the case of WF, the asymmetric  $E(\phi)$  curve (Fig. 2) is continuous at  $\phi = 0$  and the canting of the atomic moments can be predicted with certainty. This canted WF ground state can be calculated directly using the density-functional-theory (DFT) codes consistently treating both SOC and noncollinear magnetic configurations. Indeed, the calculation started with the achiral collinear antiferromagnetic structure immediately reveals its instability resulting in the canting of the atomic moments [16]. The converged iterative process of the DFT calculation provides the direction of the canting (chirality), the value of the canting angle, and the energy of the corresponding chiral state.

For the RS, the direct first-principles calculation is less feasible. Compared with the case of the WF, here there are two important aspects. First, the collinear achiral magnetic structure corresponding to  $\mathbf{q} = 0$  is periodic with the periodicity of the chemical lattice whereas the spiral structures with nonzero  $\mathbf{q}$  do not have this periodicity. Therefore, the collinear state has additional symmetry and is computationally stable [32]: the collinear structure does not transform into the spiral in the iterative DFT calculations, also in the case that spiral structure has lower energy. Second, the energy curve  $E(\mathbf{q})$  is not continuous at  $\mathbf{q} = 0$  [4]. The reason for the discontinuity is the magnetic anisotropy in the plane orthogonal to the rotation axis of the spiral. In the ferromagnetic (FM) configuration ( $\mathbf{q} = 0$ ), all moments are directed along the easy axis whereas in the spiral with arbitrary nonzero wave vector  $\mathbf{q}$  the directions of the atomic moments vary with respect to the crystallographic axes averaging the energies of the easy and hard directions. Therefore, for a plane spiral structure the energy of the ferromagnetic state is by  $\frac{1}{2}(E_{\text{easy}} - E_{\text{hard}})$  lower than the limit of the spiral energy  $E(\mathbf{q})$  for  $\mathbf{q}$  tending to zero (Fig. 2). As a result, the ground-state magnetic configuration is determined by the interplay of the DMI and in-plane magnetic anisotropy. The symmetry constraint of periodicity does not allow a direct DFT calculation of the ground state of the RS. Therefore, to establish the ground magnetic state of the system, one needs to determine the curve  $E(\mathbf{q})$ .

In this paper, our main focus is on the study of the DMI through first-principles calculations of the  $E(\mathbf{q})$  function. The concrete calculations will be performed for the Co/Pt bilayer. We will consider spiral structures

$$\hat{\mathbf{S}}_i = [\sin \theta \cos(\mathbf{q} \cdot \mathbf{a}_i), \sin \theta \sin(\mathbf{q} \cdot \mathbf{a}_i), \cos \theta] \quad (3)$$

with the axis of the spiral parallel to the  $z$  axis. Here  $\mathbf{a}_i$  is the atomic position of the  $i$ th atom and  $\mathbf{q}$  is the wave vector of the spiral. We will mostly be interested in plane spiral structures with  $\theta = \frac{\pi}{2}$  and vector  $\mathbf{q}$  parallel to the  $xy$  plane. Such spiral structures are often referred to as cycloids. This type of the magnetic structure is found in magnetic thin films [33–35]. The DMI energy can be estimated through the evaluation of the energy difference between spirals with wave vectors  $\mathbf{q}$  and  $-\mathbf{q}$ :

$$E_{\text{DMI}}(\mathbf{q}) = E(\mathbf{q}) - E(-\mathbf{q}). \quad (4)$$

In terms of interatomic DMI parameters  $\mathbf{D}_{ij}$ , the DMI energy takes the form

$$E_{\text{DMI}}(\mathbf{q}) = 2(-\sin \theta \cos \theta \mathbf{e}_x + \sin^2 \theta \mathbf{e}_z) \cdot \sum_j \mathbf{D}_{0j} \sin(\mathbf{q} \cdot \mathbf{a}_j), \quad (5)$$

where  $\mathbf{e}_x, \mathbf{e}_z$  are unit vectors in the directions of the  $x$  and  $z$  axes. For small  $\mathbf{q} = (q, 0, 0)$  vectors parallel to the  $x$  axis and  $\theta = \frac{\pi}{2}$ , expression (5) simplifies into

$$E_{\text{DMI}}(q) = 2q \sum_j D_{0j,z} a_{j,x} = qD, \quad (6)$$

where

$$D = 2 \sum_j D_{0j,z} a_{j,x}. \quad (7)$$

Calculating  $E_{\text{DMI}}(\mathbf{q})$  for vectors  $\mathbf{q}$  sampling the whole Brillouin zone (BZ), one can estimate the values of the interatomic DMI parameters using the procedure similar to the frozen-magnon approach for the calculation of the Heisenberg interatomic exchange parameters [36,37]. In this paper, we will mostly focus on the estimation of the cumulative parameter  $D$ .

### III. METHODS OF THE CALCULATION OF THE DMI ENERGY OF THE RELATIVISTIC SPIRALS

To estimate the DMI energy from the difference  $E(\mathbf{q}) - E(-\mathbf{q})$ , we need to know function  $E(\mathbf{q})$ . The calculation of the energy of the system as a function of continuous parameter  $\mathbf{q}$  is a nontrivial task. As mentioned above, a straightforward possibility is to perform the supercell calculations. Selecting a value of  $\mathbf{q}$  that is commensurate with the periodicity of the atomic lattice, we can perform calculations for  $\mathbf{q}$  and  $-\mathbf{q}$  spirals in the supercell whose size is determined by the wavelength of the spiral. The disadvantage of this approach is a strong dependence of the size of the supercell on vector  $\mathbf{q}$ . For example, for a very small commensurate  $\mathbf{q}$ , the supercell is huge that demands for extensive computer resources and makes difficult to achieve the desired numerical accuracy of the energy difference  $E(\mathbf{q}) - E(-\mathbf{q})$ . We will apply the supercell calculation for a selected  $\mathbf{q}$  value. The main purpose of applying the supercell method in this paper is to test the results of the much faster and more convenient approach suggested below.

This alternative calculation strategy arises from the idea of employing the concepts of the generalized translational symmetry and generalized Bloch function [17,30] for the study of the DMI. In the *nonrelativistic and scalar-relativistic* DFT calculations, the Kohn-Sham Hamiltonian of the spiral is symmetric under the operations of the generalized translations that combine the usual space translations and spin rotations [30]. This symmetry allows to reduce, in an exact manner, the calculation of the spiral with arbitrary wave vector  $\mathbf{q}$  to the consideration of the small  $\mathbf{q}$ -independent chemical unit cell. However if the SOC is not taken into account,  $E(\mathbf{q}) = E(-\mathbf{q})$  and there is no DMI. The inclusion of the SOC into consideration destroys the symmetry of the Kohn-Sham Hamiltonian with respect to the generalized translations and therefore does not allow an exact reduction of the relativistic calculations to the chemical unit cell [38].

On the other hand, under some approximations the application of the generalized Bloch functions for the calculation of the DMI energy is possible. Heide *et al.* [23] suggested to consider SOC as small perturbation and calculate the first-order perturbation energy for the states of the nonrelativistic spiral [24]. They have shown that within first-order perturbation theory for plane spiral structures the matrix elements of in-plane components of the SOC operator are zero and the matrix elements of the  $z$  component of the SOC provide the nonvanishing contributions to the energy. Since these contributions are different for  $\mathbf{q}$  and  $-\mathbf{q}$  spirals, their sums over occupied electronic states give an estimation of the DMI energy.

In this paper, we suggest a different method based on the use of the generalized Bloch functions. In our opinion, this method has some advantages with respect to the approach used by Heide *et al.* Instead of dealing with the perturbation

energy of the individual electronic states of the nonrelativistic spiral, we consider the Hamiltonian

$$H = H_{sc} + H_{SO}^z \quad (8)$$

where  $H_{sc}$  is the scalar-relativistic Hamiltonian of the spiral structure in the atomic-sphere approximation (see, e.g., Ref. [17] for details) and  $H_{SO}^z$  is the  $z$  component of the SOC operator

$$H_{SO}^z = \frac{1}{(2c)^2} \frac{1}{rM^2} \frac{dV^{av}}{dr} \sigma_z \hat{l}_z, \quad (9)$$

where

$$V^{av}(r) = \frac{1}{2}[V^+(r) + V^-(r)] \quad (10)$$

and

$$M = \frac{1}{2} \left( 1 - \frac{1}{c^2} V^{av} \right), \quad (11)$$

$\sigma_z$  is the Pauli matrix,  $\hat{l}_z$  is the operator of the  $z$  component of the orbital momentum, and  $V^{av}$  is the average of the spin-up and -down potentials. In Eqs. (9) and (11), the Rydberg atomic units are used. The SOC in the form (9) neglects the  $x$  and  $y$  components of the SOC operator presented by the  $\sigma_x \hat{l}_x$  and  $\sigma_y \hat{l}_y$  products. (The complete form of the SOC operator can be found, e.g., in Ref. [39].)

The  $H_{SO}^z$  operator is periodic and spin diagonal with respect to the  $z$  axis. We remind that the  $z$  axis is the axis of the spiral. Both  $H_{sc}$  and  $H_{SO}^z$  and therefore their sum given by Eq. (8) are invariant with respect to the generalized translations. Hence, an exact treatment of the Hamiltonian  $H$  can be performed with the use of the chemical unit cell of the system and the large BZ corresponding to the chemical unit cell.

The secular matrix of the method is the sum of the secular matrix of the scalar-relativistic spiral [17] and the matrix of the operator  $H_{SO}^z$  in the basis of generalized Bloch functions. These two parts of the secular matrix initiate different trends in the formation of the electronic states. The scalar-relativistic spin-spiral Hamiltonian  $H_{sc}$  leads to the mixing of the spin-up and -down states with Bloch wave vectors shifted by vector  $\mathbf{q}$  in the reciprocal space. The strength of the mixing depends on the value of the cone angle  $\theta$  in Eq. (3). It is the strongest for  $\theta = \frac{\pi}{2}$  and vanishes for  $\theta = 0$  and  $\pi$  corresponding to collinear magnetic structures. As mentioned above, in this paper we mostly focus on the plane cycloidal spirals corresponding to  $\theta = \frac{\pi}{2}$  and maximal spin mixing.

The second term,  $H_{SO}^z$ , stimulates the energy shift of the electronic states with the direction of the shift depending on the spin projection of the state on the  $z$  axis. Since the electronic states are spin mixed, operator  $H_{SO}^z$  stimulates different directions of the energy shifts for different spin components of the electronic state. The direction and value of the energy shift depend also on the spatial form of the wave function because of the  $l_z$  operator in the expression for  $H_{SO}^z$  that stimulates opposite energy shifts for the spherical harmonics with opposite signs of magnetic number  $m$ . All these complex competing trends are consistently taken into account by the matrix elements of the secular matrix and are reflected in the energies and wave functions of the calculated states of the spiral obtained by the diagonalization of the secular matrix. We remark that in difference to the first-order

perturbation scheme of Heide *et al.* [23], the ASW-qSO method takes into account the modifications of the wave functions and can include the SOC in the self-consistent calculations.

There are several arguments why the neglect of the  $x$  and  $y$  components of the SOC is expected to be a good approximation for the estimation of the DMI energy of the spiral structures. First, we can refer to the consideration by Heide *et al.* [23] who have shown that the matrix elements of the  $x$  and  $y$  components of the SOC vanish for the generalized Bloch states of the scalar-relativistic Hamiltonian. Second, neglecting the  $x$  and  $y$  components we obtain somewhat different values of  $E(q)$  and  $E(-q)$  compared to the corresponding spiral energies calculated in the supercell approach with full account for the SOC. However, the difference  $E(q) - E(-q)$  identified as the DMI energy is close in both types of the calculations. The quality of the approximation can be tested by the comparison with the results of the supercell calculation with full account for the SOC. As we show below, the agreement is encouraging.

## IV. RESULTS AND DISCUSSION

### A. Details of the calculations

The calculations are performed for the Co/Pt bilayer with one atomic layer of Co on one atomic layer of Pt. In Fig. 3 we show the geometry of the bilayer and the plane of the cycloidal spiral structures. The spin-quantization axis  $z$  is orthogonal to the plane of the spiral. The lattice parameter of the in-plane hexagonal lattice is  $a = 5.24$  au that corresponds to the lattice parameter of 7.41 au of the bulk fcc Pt. The distance between Pt and Co layers is 3.89 au. To simulate vacuum, four layers of the empty spheres were included.

The calculations are performed with the augmented spherical wave (ASW) method [40,41]. The description of the account for the noncollinear magnetism and SOC within the framework of the ASW method can be found in Ref. [17]. To the version of the ASW method dealing with the Hamiltonian given by Eq. (8), we will refer as ASW-qSO.

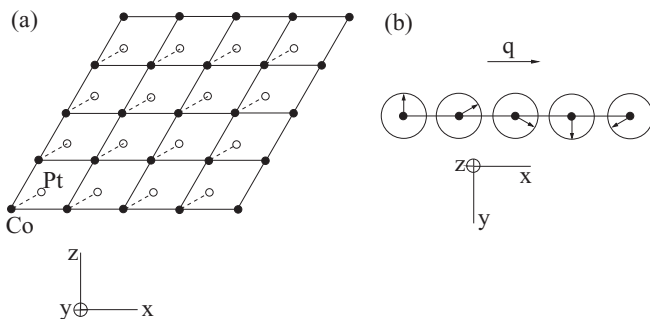


FIG. 3. (a) The geometry of the Co/Pt bilayer. The atomic positions of the Co layer are shifted with respect to the atomic positions of the Pt layer. The  $y$  axis is orthogonal to the film. (b) Schematic picture of the cycloidal spiral structure with atomic moments parallel to the  $xy$  plane and wave vector of the spiral parallel to the  $x$  axis. The  $z$  axis is directed into the plane of the figure. The spiral with positive (negative)  $q$  value corresponds to the clockwise (anticlockwise) spin configuration in terms of Ref. [26].

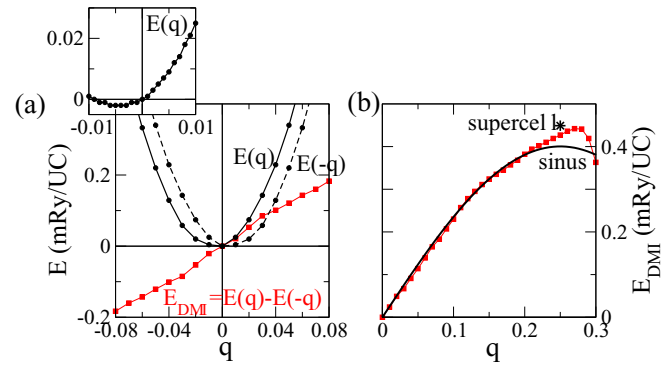


FIG. 4. (a) Solid black curve shows function  $E(q)$  calculated with the ASW-qSO method. The broken curve presents  $E(-q)$  function. The red line gives the DMI energy as a function of  $q$  obtained as  $E_{\text{DMI}}(q) = E(q) - E(-q)$ . The inset in the upper-left part of the panel shows  $E(q)$  calculated with a finer mesh for a smaller  $q$  interval from  $-0.01$  to  $0.01$ . (b) Red curve with square symbols shows  $E_{\text{DMI}}(q)$  for a larger  $q$  interval up to  $q = 0.3$ . The black curve is a sinusoid. The asterisk presents the result of the supercell calculation for  $q = 0.25$ . For the sake of comparison, all energies are given per chemical unit cell containing one Co atom.

### B. DMI energy from the ASW-qSO calculation

In Fig. 4(a) we show  $E(q)$  in the interval of  $q$  from  $-0.08$  to  $0.08$  calculated with the ASW-qSO method for vectors  $\mathbf{q}$  parallel to the  $x$  axis. In the paper the value of  $q$  is always given in units of  $\frac{2\pi}{a}$ . The energy origin is selected at the energy of the FM structure. The asymmetry of  $E(q)$  with respect to the sign reversal of  $q$  is clearly seen. Zooming into the region of small values of  $q$  [inset to Fig. 4(a)] shows, in agreement with general arguments above, negative values of  $E(q)$  for small negative  $q$ . Therefore, the minimum of  $E(q)$  is not at  $q = 0$  and does not correspond to the collinear magnetic structure. The difference  $E(q) - E(-q)$  appears to be close to a straight line in this  $q$  interval, demonstrating that one  $q$ -independent  $D$  parameter describes well the DMI energy in a broad  $q$  interval. The property for positive  $q$  values  $E(q) > E(-q)$  agrees with the conclusion of Ref. [26] about anticlockwise type of the spiral structure.

In Fig. 4(b) we present the DMI energy calculated for  $q$  values up to 0.3. As expected, in this larger  $q$  interval the deviation of  $E_{\text{DMI}}(q)$  from a linear dependence is well seen. However, in a broad  $q$  interval up to about 0.23, the dependence is very well described by one sinusoid with period of 1 [Eq. (5)]. For  $q$  from 0.23 up to 0.3, the deviation from a simple sinusoid becomes substantial. This change in the character of the  $q$  dependence can be interpreted as involvement for these large  $q$  values of new groups of electronic states in intense hybridization. Below (Fig. 16, Sec. IV H), we will consider DMI energy for several model calculations and see that, in general, the strong deviation from simple dependence may appear for much smaller  $q$  values. In terms of effective Hamiltonian of interacting atomic moments, the deviation from the simple sine function means the necessity to include the interatomic interactions beyond the nearest-neighbor interactions [see Eq. (5)]. The asterisk in the right panel shows the value of the DMI energy calculated with

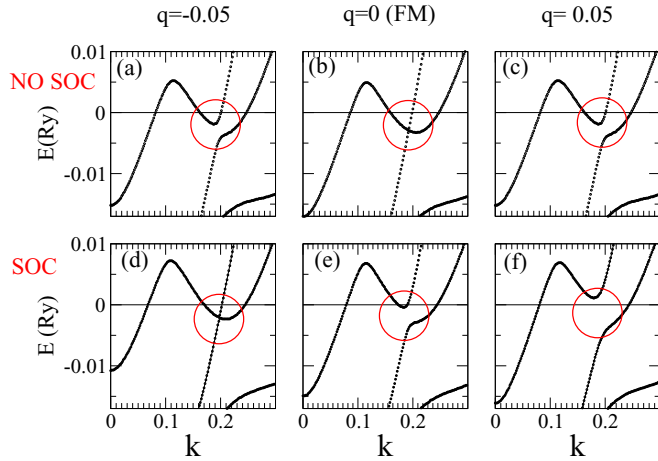


FIG. 5. The fragment of the band structure for six physical cases. The upper panels [(a)–(c)] show the results of the scalar-relativistic calculations, the lower panels [(d)–(f)] present the results of the calculations with the ASW-qSO method. The panels (b) and (e) correspond to the ferromagnetic structure with  $q = 0$ , the other four panels correspond to the spiral structures with  $q = \pm 0.05$ . Encircled are the regions of the avoided crossing where the strongest change in the band structure is observed. In agreement with symmetry arguments, the band structures of the  $\pm q$  spirals are identical in the scalar-relativistic calculation and strongly different in the ASW-qSO calculation.

the supercell approach for  $q = 0.25$ . Obviously, the agreement between two methods is very good.

To compare our value of  $E_{\text{DMI}}$  from the supercell calculation for  $q = 0.25$  with corresponding value  $d^{\text{tot}}$  from Ref. [26], we should divide it by three and transform to meV. The obtained value is 2.0 meV. The corresponding value that we can read from Fig. 2 of Ref. [26] is  $d^{\text{tot}} = 1.5$  meV. According to the erratum to Ref. [26], this value should be multiplied by  $\sqrt{3}$  what gives  $d^{\text{tot}} \approx 2.6$  meV. Taking into account the difference in the calculation techniques and, possibly, in the lattice parameters the values are in fair agreement with each other. The lattice parameters of the relaxed lattice are not given in Ref. [26].

### C. Reciprocal-space analysis of the contributions to the DMI energy

To understand the microscopic origin of the DMI, it is instructive to examine the properties of the band structures of different magnetic configurations. In Fig. 5 we show a small fragment of the band structure for six different physical cases: the ferromagnetic configuration and the spiral structures with wave vectors  $q = \pm 0.05$  calculated with both scalar-relativistic Hamiltonian [Figs. 5(a)–5(c)] and with the Hamiltonian of the ASW-qSO method [Figs. 5(d)–5(f)]. As expected on the basis of symmetry arguments, in the scalar-relativistic calculations the band structures of the  $\mathbf{q}$  and  $-\mathbf{q}$  spirals are identical, leading to vanishing DMI energy. On the other hand, the ASW-qSO calculations result in the distinctly different band structures of the  $\pm \mathbf{q}$  spirals [Figs. 5(d) and 5(f)].

In the figures we encircle the region of the strongest variation of the band structure. This is the region of so-called

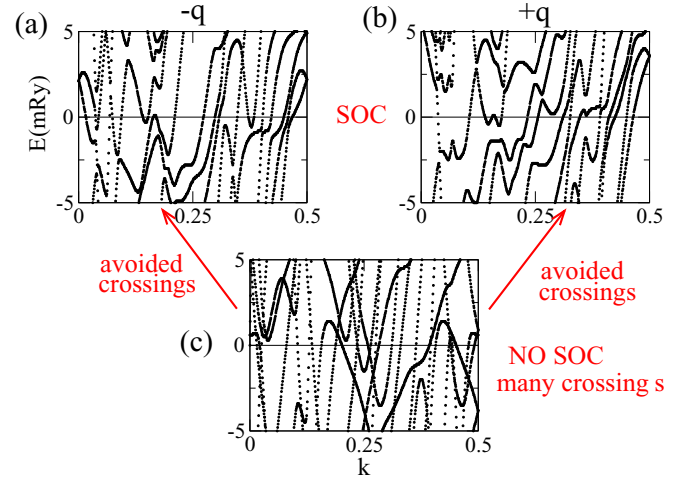


FIG. 6. The fragment of the band structure calculated within the supercell approach. The size of the supercell corresponds to the wave vector  $q = 0.25$ . (c) FM structure, scalar-relativistic calculation; (a) spiral with  $q = -0.25$ , ASW-qSO calculation; (b) spiral with  $q = 0.25$ , ASW-qSO calculation.

avoided crossing or anticrossing of the energy bands. In the scalar-relativistic ferromagnetic structure, two bands cross each other [Fig. 5(b)]. This is the case of the highest symmetry between the six physical situations shown in the figure. In all other cases, the decreased symmetry leads to the hybridization of the states of the intersecting bands. In Figs. 5(a) and 5(c) we see strong hybridizational repulsion of the bands in the scalar-relativistic calculation for spirals with nonzero wave vectors. The hybridizational repulsion is the strongest around the intersection point where the energies of the interacting states are close to each other.

The account for the SOC decreases the symmetry already in the FM state [Fig. 5(e)] and leads to the mixing and hybridizational repulsion of the bands. The most important is that, in contrast to the scalar-relativistic case, the variation of the band structure with respect to the FM case is different for  $\mathbf{q}$  and  $-\mathbf{q}$  spirals [Figs. 5(d) and 5(f)]. In the case of  $q = 0.05$ , the states of the two bands become closer to each other [Fig. 5(d)] than in the FM case; in the case of  $q = -0.05$  the energy distance between the states increases further [Fig. 5(f)]. Thus, the influences of the SOC and noncollinearity of the spin structure are enhancing each other in one case [Fig. 5(f)] and compensating each other in the other case [Fig. 5(d)]. The difference in the electronic states of the magnetic configurations with opposite chirality is the essence of the DMI. It is worth noting that an apparent intersection of the bands in the circle in Fig. 5(d) in reality does not take place. Strong zooming into this region shows that also here the bands do not cross. The avoiding of the crossing happens very sharp in a very narrow  $k$  and energy interval. This feature is in agreement with results of previous studies [25,27]. On the other hand, in the scalar-relativistic FM case [Fig. 5(b)] the intersection indeed takes place.

The processes shown in Fig. 5 are clearly seen also in the band structures obtained in the supercell calculations (Fig. 6). The supercell corresponds to the periodicity of the spiral with

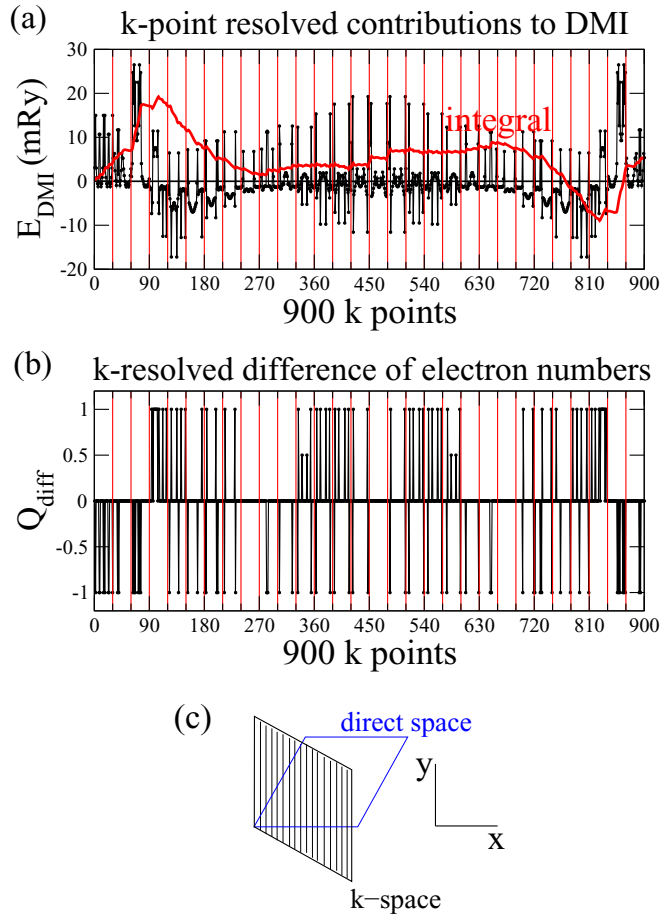


FIG. 7. (a)  $\mathbf{k}$ -resolved contributions to the DMI energy calculated with the ASW- $q$ SO method for spirals with  $q = \pm 0.05$ . The red line corresponds to the numerical integration over the  $\mathbf{k}$ -points mesh. (b)  $\mathbf{k}$ -resolved difference in the number of the occupied states for spirals with  $q = \pm 0.05$ . (c) The 900  $\mathbf{k}$  points used in panels (a) and (b) uniformly fill the 2D unit cell in the reciprocal space. The sequence of the points in the  $\mathbf{k}$  mesh corresponds to the sequence of the straight lines parallel to the  $y$  axis in this panel. There are 30 straight lines with 30 points on each of them.

$q = 0.25$ . Since in this case the BZ is smaller, the number of bands correspondingly increases. The scalar-relativistic calculation gives a large number of the band crossings [Fig. 6(c)]. Most of them disappear in the relativistic calculations for the spiral structures forming numerous avoided crossings [Figs. 6(a) and 6(b)]. Again, there is clear difference between band structures of the spirals with opposite chirality. We remark that in the supercell calculation shown in Fig. 6 we used the wave vector whose length is five times larger than the length of the wave vector used in the ASW- $q$ SO calculation shown in Fig. 5. The supercell calculation with  $q = 0.05$  needs a much larger supercell and the number of the bands strongly increases further.

In Fig. 5 we present only one small fragment of the electronic structure calculated with the ASW- $q$ SO method. A more complete picture of the contributions of different  $\mathbf{k}$  points of the reciprocal space to the DMI energy is given in Fig. 7(a). Here, we show for the case of  $q = 0.05$  the differences  $E_{\text{DMI}}(\mathbf{k}|q) = E(\mathbf{k}|q) - E(\mathbf{k}|-q)$  for 900 points

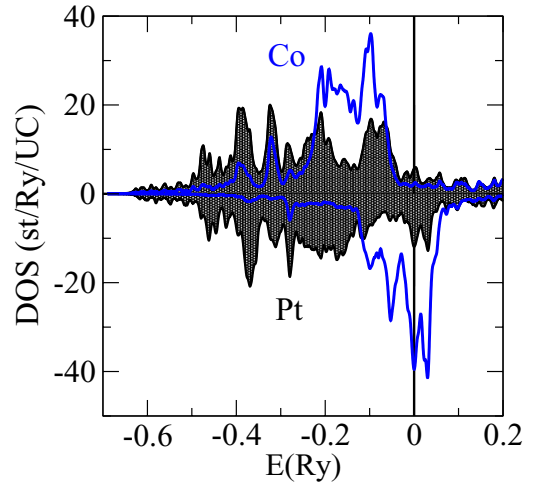


FIG. 8. Partial atomic DOSs of Co (blue curves) and Pt (black filled curves) calculated for the ferromagnetic structure. Above the abscissa axis are the spin-up DOSs, below the abscissa axis are the spin-down DOSs.

in the unit cell of the reciprocal lattice. The  $\mathbf{k}$  points are uniformly distributed over the 30 lines parallel to the  $y$  axis [Fig. 7(c)]. The strongly fluctuating behavior of the  $\mathbf{k}$ -resolved contributions is determined by the varying local properties of the band structures of the two spirals with opposite chirality. In particular, the closeness of the avoided-crossing points to the Fermi energy and corresponding strong repulsion of the energy states can bring some of the states above the Fermi level. This results in different numbers of the occupied bands at a given  $\mathbf{k}$  point for the  $\mathbf{q}$  and  $-\mathbf{q}$  spirals and, correspondingly, in stronger contribution to the DMI energy. Since, however, the total number of electrons is conserved, the increased occupation of the electronic states for the  $\mathbf{q}$  spiral at a given point  $\mathbf{k}$  leads to an increased occupation for the  $-\mathbf{q}$  spiral at another  $\mathbf{k}$  point. In Fig. 7(b) we present the  $\mathbf{k}$ -resolved difference in the number of occupied states  $Q_{\text{diff}}(\mathbf{k}|q) = Q(\mathbf{k}|q) - Q(\mathbf{k}|-q)$  where  $Q(\mathbf{k}|q)$  is the number of the occupied states at point  $\mathbf{k}$  for the spiral with wave vector  $q$ . There is correlation between the deviations of the  $Q_{\text{diff}}(\mathbf{k})$  from zero [Fig. 7(b)] and the strong features in  $E_{\text{DMI}}(\mathbf{k})$  [Fig. 7(a)]. The fluctuations of the contributions of the individual  $\mathbf{k}$  points considerably compensate each other in the integral quantity [see red line in Fig. 7(a)].

#### D. Role of the Co-Pt hybridization

The consideration above, in particular the contribution of the avoided-crossing points in the electronic structure to the DMI energy, reveal the importance of the hybridizational processes in the electronic structure. It is of special interest to investigate the role of the Co-Pt hybridization since such a hybridization suggests an important channel of connecting different physical components crucial for the DMI: spin degrees of freedom of the Co subsystem and strong SOC of the Pt subsystem.

At the first stage we inspect the partial Co and Pt DOSs (Fig. 8). The presence of the Co-Pt hybridization is seen through numerous common peak and deep structures that

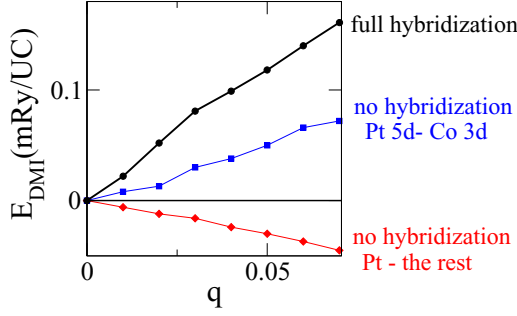


FIG. 9. The  $E_{\text{DMI}}(q)$  dependencies calculated under different assumptions on the character of the interatomic hybridization: (1) the neglect of the hybridization of the Pt  $5d$  and Co  $3d$  basis ASW functions (blue curve, square symbols), (2) the neglect of the hybridization of the all Pt basis ASW functions with other basis functions (red curve, diamond symbols), (3) full calculation (black curve, circle symbols).

reveal the origin of these structures from the same hybridized electronic states.

To study the impact of the Co-Pt hybridization on the DMI, we performed two model calculations with the ASW-qSO method neglecting either the hybridization between Pt  $5d$  and Co  $3d$  basis ASW functions or the hybridization of all Pt ASW basis functions with the rest of the system. The neglect of the hybridization was introduced in the calculation by setting to zero the matrix elements of the Hamiltonian and overlap matrices on the corresponding ASW basis functions. The results of the calculation are presented in Fig. 9. We see that in the first case the slope of the  $E_{\text{DMI}}(q)$  decreased by roughly 50% and in the second case it changed the sign and further strongly decreased in the absolute value. These model calculations very clearly demonstrate the importance of the Co-Pt hybridization in the electronic states for the DMI strength [42]. The conclusion of the importance of the interatomic hybridization for the DMI agrees with the results of the tight-binding-model study reported in Ref. [43].

### E. Real-space distribution of the DMI energy

To address the problem of the location of the DMI energy in the real space we need to calculate the distribution of the DMI energy over atomic spheres. This is done as follows. The ASW method employed in our calculations, as many other DFT methods, provides both electronic energies  $\epsilon_{\mathbf{k}n}$  and corresponding electronic wave functions  $\psi_{\mathbf{k}n}(r)$ . The wave functions are normalized to unity in the unit cell

$$\int_{\Omega_{UC}} \psi_{\mathbf{k}n}(r)^\dagger \psi_{\mathbf{k}n}(r) dr = 1, \quad (12)$$

where the integral is taken over the volume of the unit cell. This unity is distributed over the atomic spheres according to the shape of the wave function:  $\sum_{\nu} Q_{\mathbf{k}n}^{\nu} = 1$  where

$$Q_{\mathbf{k}n}^{\nu} = \int_{\Omega_{\nu}} \psi_{\mathbf{k}n}(r)^\dagger \psi_{\mathbf{k}n}(r) dr \quad (13)$$

and  $\Omega_{\nu}$  denotes the  $\nu$ th atomic sphere. The portion  $\epsilon_{\mathbf{k}n} Q_{\mathbf{k}n}^{\nu}$  of the energy of a given state ( $\mathbf{k}n$ ) can be assigned to the  $\nu$ th atomic sphere. The sum  $E_{\nu} = \sum_{\epsilon_{\mathbf{k}n} \leq E_F} \epsilon_{\mathbf{k}n} Q_{\mathbf{k}n}^{\nu}$  over occupied

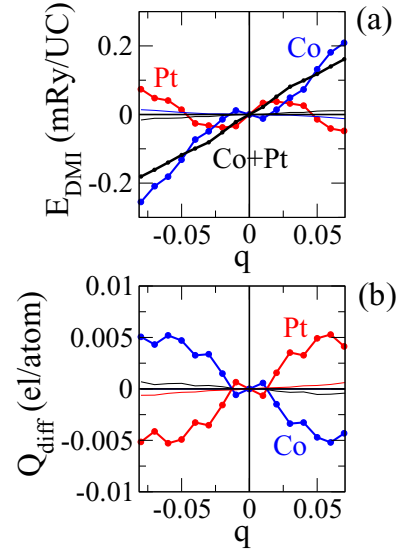


FIG. 10. (a)  $q$  dependence of the atom-resolved contributions to the DMI energy. Blue (red) line shows Co (Pt) contribution. The black line presents the sum of the Co and Pt contributions. (b)  $q$  dependence of the atom-resolved redistribution of the electronic density between  $\mathbf{q}$  and  $-\mathbf{q}$  spirals. In both panels, the lines close to the abscissa axis correspond to the small contributions from the empty spheres simulating vacuum region.

states gives the contribution of the atom  $\nu$  to the energy of the system. The difference of the atomic energies calculated for  $\mathbf{q}$  and  $-\mathbf{q}$  spirals provides the contribution of the  $\nu$ th sphere to the DMI energy.

In Fig. 10(a) we plot the atom-resolved contributions to the DMI energy. We obtained an interesting result that the  $q$  dependencies of the atom-resolved contributions are nonmonotonic for both Co and Pt. The linear pieces connecting the values of the functions at neighboring points of the  $q$  mesh have the slopes strongly varying from  $q$  interval to  $q$  interval. It is remarkable, however, that in the total  $E_{\text{DMI}}(q)$  the peculiar features of the Co and Pt contributions compensate each other resulting in an almost perfect straight line.

To shed light on the physical origin of this behavior, we consider the  $q$ -dependent redistribution of the electronic density between Co and Pt atoms for  $\mathbf{q}$  and  $-\mathbf{q}$  spirals  $Q_{\text{diff}}^{\nu}(q) = Q^{\nu}(q) - Q^{\nu}(-q)$  [Fig. 10(b)]. The corresponding piecewise linear functions have the features strongly correlated with the features of the atom-resolved energy functions [Fig. 10(a)]. Since the total electronic number is the same for all spirals, the both partial curves of the charge differences are approximately opposite and their sum is close to zero for all  $q$  values. (The small deviation from zero results from small contributions of the empty spheres in the vacuum region.) The  $q$ -dependent difference in the charge distribution between the spirals with opposite  $q$  vectors results in the corresponding  $q$  dependence of the atomic contributions to the DMI energy. These specific features of the atomic contributions compensate each other in the total DMI energy.

We remark that the peculiar  $q$  dependence of the atom-resolved DMI contributions could not be obtained in the calculations of the ‘‘atom-resolved spin-orbit matrix elements’’

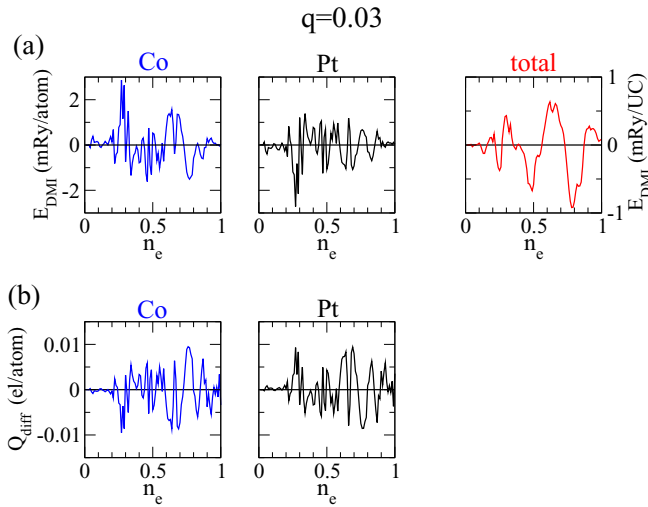


FIG. 11. (a) The atom-resolved contributions to the DMI energy and the total  $E_{\text{DMI}}$  as functions of the band occupation  $n_e$  for  $q = 0.03$ . (b) Corresponding dependence of the atom-resolved charge redistribution  $Q_{\text{diff}}(n_e)$ .

reported in Ref. [23] using the unperturbed wave functions of nonrelativistic spirals. Neglecting the modification of the wave functions, one neglects the effects of charge redistribution caused by the SOC.

These results show that the real-space atomic distribution of the DMI energy is strongly  $\mathbf{q}$  dependent in contrast to the total DMI energy that is much less sensitive to the variation of the magnetic configuration. The strong dependence of the atomic contributions on the wave vector  $\mathbf{q}$  and the strong compensation of the features of the partial contributions in the total DMI energy demonstrate that these features should be treated as complex consequences of the hybridizational processes in the electronic structure playing a primary role in the formation of the DMI energy. Further calculational data presented below support the validity of these conclusions.

#### F. DMI as a function of the number of electrons

To gain further insight into the formation of the DMI, we consider  $E_{\text{DMI}}$  as a function of band occupation. For each value of  $Q_e$  we, keeping the electronic structure unchanged, determine the position of the Fermi level and calculate the band energy of the occupied states.

In Fig. 11 we present for the case of  $q = 0.03$  the dependence of partial atomic contributions to the DMI energy and the total  $E_{\text{DMI}}$  [Fig. 11(a)] as well as the corresponding charge transfer quantities [Fig. 11(b)] as functions of  $n_e = Q_e/Q_t$ . In Fig. 12 we present the same type of data for the case of  $q = 0.25$ .

The  $n_e$ -dependent quantities for both  $q$  values confirm the conclusions derived in the previous section for the  $\mathbf{q}$  dependence of the quantities considered for the actual electron number corresponding to  $n_e = 1$  (Fig. 10). The atomic DMI energy contributions fluctuate strongly with the variation of the number of electrons [Figs. 11(a) and 12(a)]. These oscillations correlate with the oscillations in the  $n_e$  dependencies of the atomic redistribution of the electronic

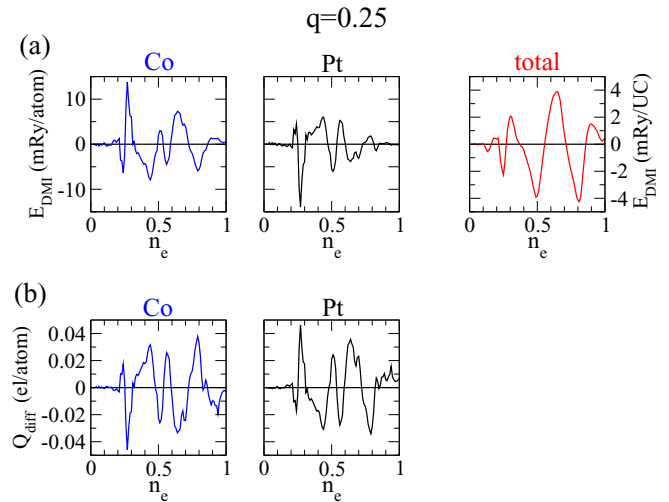


FIG. 12. The same as in Fig. 11 but for  $q = 0.25$ .

charge differences [Figs. 11(b) and 12(b)]. The sum of the atomic contributions to  $E_{\text{DMI}}(n_e)$  for both  $q$  presented is considerably smoother than the corresponding atomic contributions themselves [Figs. 11(a) and 12(a)]. This result shows again that many features of the partial atomic contributions strongly compensate each other and, therefore, these features are of limited physical significance for the interpretation of the total DMI energy.

For the case of  $q = 0.25$  we performed the calculations of the  $n_e$ -dependent quantities also with the supercell method. The results obtained in this calculation are similar to those shown in Fig. 12 and we do not present them. The total  $E_{\text{DMI}}(n_e)$  calculated with the supercell method is presented for comparison in Fig. 13.

Another important feature obtained in the calculation of the  $n_e$  dependencies is the similarity in the shapes of  $E_{\text{DMI}}(n_e)$  curves calculated for different  $q$  values (Fig. 13). The increase of  $q$  leads to the expected increase of the amplitude of the

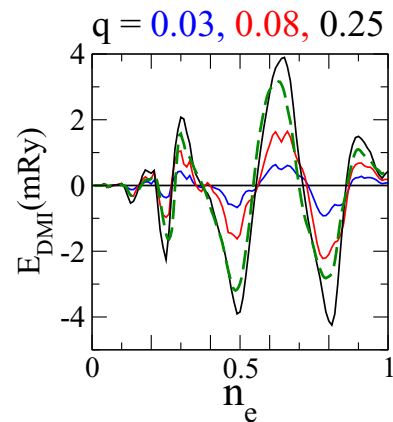


FIG. 13.  $E_{\text{DMI}}(n_e)$  calculated for different values of  $q = 0.03, 0.08, 0.25$  with the ASW-qSO method (solid curves). Increasing amplitude of the curves corresponds to the increasing  $q$  value. For comparison, the  $E_{\text{DMI}}(n_e)$  calculated with the supercell approach for  $q = 0.25$  is also shown (broken line).

peaks. In addition, for large  $q = 0.25$  there is less fine structure in the peaks. Otherwise, the positions and signs of the peaks are identical for a broad range of  $q$  values.

This behavior can be explained as follows. The spiral structure leads to the hybridization of the electronic states of the ferromagnetic configuration that are separated by vector  $\mathbf{q}$  in reciprocal space [17]. Therefore, for larger  $\mathbf{q}$  the hybridization involves the states from larger regions of the reciprocal space. Also, the strength of the hybridization increases with increasing  $\mathbf{q}$  since the off-diagonal matrix elements of the secular matrix responsible for the hybridization increase with increasing  $\mathbf{q}$ . Indeed, these matrix elements contain the differences of the structure constants between reciprocal space points separated by vector  $\mathbf{q}$ . The details of the hybridization are different for  $\mathbf{q}$  and  $-\mathbf{q}$  spirals giving rise to the DMI. The similarity of the  $E_{\text{DMI}}(n_e)$  curves calculated for different  $\mathbf{q}$  shows that for broad  $\mathbf{q}$  interval, the states involved into hybridization and the character of the hybridization are qualitatively similar, differing in the quantitative characteristics of the number of states involved into intense hybridization and the strength of the hybridization. This qualitative similarity is the origin of the simple sinusoidal form of the  $E_{\text{DMI}}(q)$  dependence in a broad  $q$  interval presented in Fig. 4. For larger  $\mathbf{q}$ , the states involved into hybridization can become principally different that leads to considerable complication of the  $E_{\text{DMI}}(q)$  curve [see Fig. 16(b) and corresponding discussion below]. To deal with such complications, one needs to introduce the  $q$  dependence of the effective nearest-neighbor DMI parameter or to consider longer-range interatomic DMI interactions or to deal with more complex forms of antisymmetric interactions of atomic moments.

In addition to the  $E_{\text{DMI}}(n_e)$  dependencies calculated with the ASW-qSO method for three different  $q$  values, we show in Fig. 13 this dependence obtained with the supercell calculation for  $q = 0.25$ . The corresponding functions  $E_{\text{DMI}}(n_e)$  obtained with both methods are in good agreement.

### G. Relation between induced Pt moment and DMI strength

Ryu *et al.* [29] analyzed their measurements of the velocity of the current driven motion of the domain walls in Co film grown on different substrates of nonmagnetic heavy elements and arrived at the conclusion that the strength of the DMI in the magnetic film is in direct relation to the value of the induced moment in the nonmagnetic substrate. Yang *et al.* [26] challenged this conclusion. They performed calculations imposing constraint on the value of the Pt spin moment and have shown that decrease of the Pt moment to zero can even lead to an increase of the DMI.

We also performed calculation with constraint on the Pt moment aiming to compare our results with those reported by Yang *et al.* and to relate these results to the conclusions derived in the earlier parts of this paper. The constrained calculation was performed by applying the constraining magnetic field to the Pt atoms [44,45]. The value of the field of 21 mRy in energy units was determined for the FM structure under the condition on the Pt spin moment  $m_{\text{Pt}} = 0$ . Although the induced Pt moment in the constrained calculation is zero, the inspection of the spin-projected Pt DOS (Fig. 14) shows that the difference

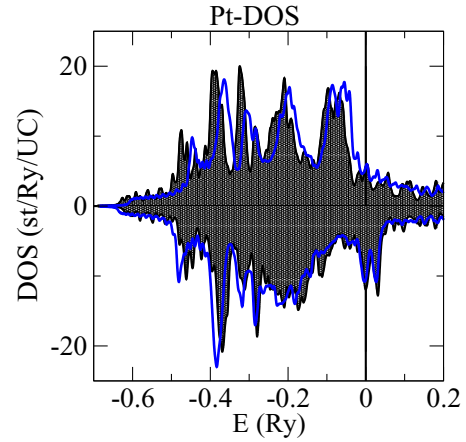


FIG. 14. The comparison of the spin-projected Pt-DOSs calculated with the constraint  $m_{\text{Pt}} = 0$  (blue curves) and without constraint (black filled curves). The calculations are performed for the ferromagnetic structure. The unconstrained value of the Pt moment is  $m_{\text{Pt}} = 0.28 \mu_B$ .

of the Pt-DOS obtained in constrained calculation from the Pt-DOS in the unconstrained case is small. It is crucial that the Pt-DOS in the case of  $m_{\text{Pt}} = 0$  remains spin polarized. The difference between partial spin-up and -down DOSs has not considerably decreased compared to the unconstrained case. The ASW-qSO calculation of the spiral structures with the atomic potentials obtained in the constrained calculation gave the results shown in Fig. 15. We see a noticeable change in the  $E(q)$  curve with respect to unconstrained calculation (Fig. 4) but the difference  $E_{\text{DMI}}(q) = E(q) - E(-q)$  remains almost unchanged. This result shows that, in agreement with the conclusion of Yang *et al.* [26], the value of the induced Pt moment does not appear as a crucial quantity governing the strength of the DMI. On the other hand, it is very important to remark that although this integral quantity by itself is not crucial, the spin polarization of the Pt states through the hybridization with spin-polarized states of Co is an important component of the DMI formation. This crucial spin polarization of the individual electronic states is not directly reflected in the total induced Pt moment. The zero value of the induced Pt moment is the result of the compensation of the spin contributions coming from different electronic states. But, this compensation is basically the feature of the nonrelativistic

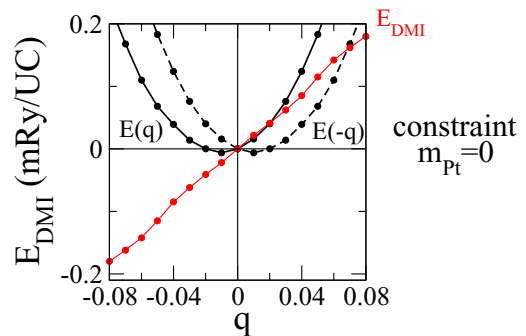


FIG. 15.  $E(q)$  and DMI energy obtained under the constraint of  $m_{\text{Pt}} = 0$ .

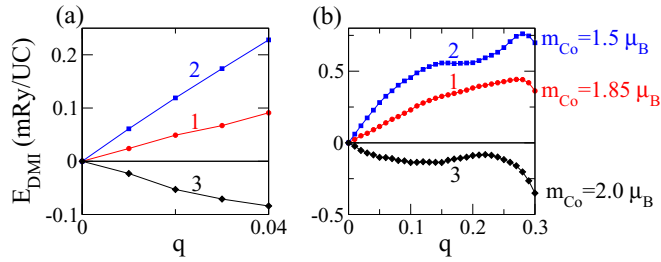


FIG. 16. The influence of the constraint on the value of the Co moment on the DMI energy as a function of spiral wave vector. The left panel (a) shows the  $E_{\text{DMI}}(q)$  curves for a small  $q$  interval. The right panel (b) shows the same curves for a larger  $q$  interval. Curve (1) corresponds to the unconstrained value of the Co moment  $m_{\text{Co}} = 1.85 \mu_B$ . Curves (2) and (3) correspond to the constrained values of the Co moment  $m_{\text{Co}} = 1.5 \mu_B$  and  $2.0 \mu_B$ , respectively.

processes that does not tell us how different is the response of the individual electronic states of the  $\pm \mathbf{q}$  spirals to the SOC. This response depends sensitively on which electronic states are close in energy and therefore participate in intense hybridization, especially if this hybridization takes place close to the Fermi level.

#### H. Relation between Co moment and DMI strength

To complete the physical picture developed in the previous sections, we consider the influence of the value of the Co moment on the DMI strength. The calculations are performed in the same way as in Sec. IV G with the only difference that the constraining field is now imposed on the Co atoms. In Fig. 16 we compare the  $E_{\text{DMI}}(q)$  functions calculated for the unconstrained value of  $m_{\text{Co}} = 1.85 \mu_B$  and constrained values of  $m_{\text{Co}} = 1.5 \mu_B$  and  $2.0 \mu_B$ . In Fig. 16(a) we consider a small  $q$  interval where all three dependencies can be well approximated by linear functions. The slope of the function is positive for the unconstrained calculation. It increases about two times for the smaller value  $1.5 \mu_B$  of the Co moment and changes sign for the larger value  $2.0 \mu_B$  of the Co moment. Therefore, also in these calculations we see the absence of a simple relation between the integral atomic characteristic of the Co moment and the DMI strength.

This conclusion receives further support if we consider the three  $E_{\text{DMI}}(q)$  functions in a larger  $q$  interval [Fig. 16(b)]. As already discussed above, the  $E_{\text{DMI}}(q)$  function of unconstrained calculation is well described by a simple sine function up to  $q$  of 0.23. On the other hand, the shape of the  $E_{\text{DMI}}(q)$  dependencies obtained for two constrained calculations are much more complex and also very different with respect to each other. This means that to describe the influence of the consequences in the changes of the electronic structure on the DMI energy, one needs to introduce different sets of the effective parameters of the interatomic DMI interaction when using Eq. (2) for the magnetic configurations strongly deviating from the ferromagnetic configuration.

#### I. Asymmetry of the magnon spectrum due to the DMI

The magnon spectrum in the systems with DMI is not a topic of this paper. However, we feel it is useful to point

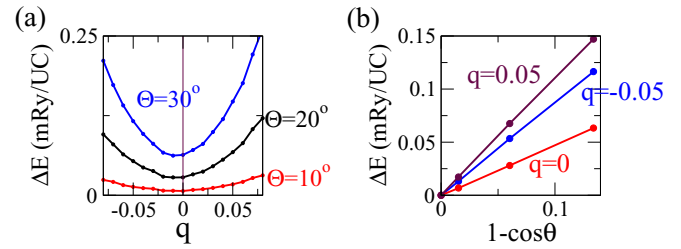


FIG. 17. (a)  $\Delta E(q, \theta) = E(q, \theta) - E(q, 0)$  as the function of  $q$  for three values of angle  $\theta$ . (b)  $\Delta E$  as a function of  $1 - \cos \theta$  playing the role of the number of magnons for three values of  $q$ .

out that the ASW-qSO method is well suited to address the asymmetry of the magnon spectrum due to the DMI. [46,47] We attract attention of the reader to the fact that the calculations considered in this section should be treated as a demonstration of the potential of the method by an application to a model system and not as a study of the real properties of a concrete physical system. In the calculation we assume that the ground state of the Co/Pt bilayer is the ferromagnetic state with the magnetization parallel to the in-plane  $z$  axis. We will show that the ASW-qSO method is able to reproduce the asymmetry of the spin-wave spectrum obtained experimentally, e.g., in the case of two layers of Fe on W(110) [47].

The magnon energy for a given  $\mathbf{q}$  can be defined as

$$\omega(\mathbf{q}) = \frac{\partial E(n_{\mathbf{q}})}{\partial n_{\mathbf{q}}}, \quad (14)$$

where  $n_{\mathbf{q}}$  is the number of magnons with wave vector  $\mathbf{q}$  and  $E(n_{\mathbf{q}})$  the corresponding energy of the system. Since  $E(n_{\mathbf{q}})$  is not symmetric with respect to the reversal of the sign of  $\mathbf{q}$ , also the magnon energies do not possess this symmetry.

We performed calculations for spiral structures with different values of  $\theta$ . In Fig. 17(a) we show  $\Delta E(q, \theta) = E(q, \theta) - E(q, 0)$  as a function of  $q$  for three different values of  $\theta$ . The curves are not symmetric with respect to the reversal of the sign of  $q$ . The number of magnons is proportional to  $(1 - \cos \theta)$ . This quantity determines the decrease of the magnetization of the system. In Fig. 17(b) we present  $\Delta E(q, \theta)$  as a function of  $(1 - \cos \theta)$  for three values of  $q = 0, \pm 0.05$ . The fact that all three dependencies have the form of practically ideal straight lines demonstrates that the description of the change of the energy of the system in terms of the number of magnons is valid for the selected intervals of  $\theta$ . The slopes of the lines give the values of the magnon energies for the corresponding wave vectors  $(q, 0, 0)$ .

Two aspects are important. First, the slopes of the lines for  $q = 0.05$  and  $-0.05$  are different, which reveals the difference of the magnon energies for the opposite values of  $q$ . This is the consequence of the DMI. Second, since the magnetic anisotropy with respect to the variation of the angle  $\theta$  is taken into account by the ASW-qSO method, the Goldstone theorem is not valid and the magnons corresponding to  $q = 0$  do not have zero energy. This feature is reflected in the nonzero slope of the line corresponding to  $q = 0$ .

## V. CONCLUSIONS

The purpose of the paper is to gain deeper insight into microscopic formation of the DMI. We aimed at the development of the physical picture able to address apparently contradicting conclusions of previous studies. The main tools of our study are the first-principles calculations of the spiral magnetic states with opposite chiralities. The value of the DMI energy is estimated as  $E_{\text{DMI}}(\mathbf{q}) = E(\mathbf{q}) - E(-\mathbf{q})$ . We applied two different methods. The first method is suggested in this paper and is based on the application of the generalized Bloch theorem and generalized Bloch functions. Since in its full form the SOC destroys the symmetry of the Hamiltonian with respect to the generalized translations, the ASW-qSO method relies on approximation in the form of the SOC. The advantages of the method are, first, the possibility to apply it to arbitrary  $\mathbf{q}$  values, second, a low demand on computer resources and, third, high numerical accuracy because of the exact reduction of the calculation to small  $\mathbf{q}$ -independent chemical unit cell. The method neglects the anisotropy in the plane orthogonal to the rotation axis of the spiral structures, which is not expected to influence importantly the DMI energy.

The second method is the supercell approach with full treatment of the SOC. The size of the supercell corresponds to the periodicity of the spiral and the method is practical only for spiral structures with rather large wave vectors commensurate with the atomic lattice. We applied both methods to the Co-Pt bilayer. The comparison of the results of the methods revealed good performance of the ASW-qSO method in the study of the DMI.

An important factor of the microscopic formation of the DMI is the hybridization between the Co and Pt atomic states. The Co states contribute with strong spin polarization and the Pt states with the consequences of strong SOC. Because of the absence of the spatial inversion in the geometry of the bilayer, the Co-Pt hybridization is different for the magnetic structures with opposite chiralities. This difference is the microscopic origin of the DMI since it leads to different energy of the electronic states and, as a result, to the different energies of the magnetic structures. The importance of the hybridizational interactions correlates directly with the conclusions of the earlier studies emphasizing the importance of the avoided crossings in the band structure for the DMI.

We considered the distribution of the DMI energy in both real and reciprocal spaces and the dependence of the DMI on the number of electrons. The results of the calculations reveal a number of energy compensations in the formation of the DMI. Thus, the partial atomic contributions as functions of  $\mathbf{q}$  are nonmonotonic and have strongly varying slopes. However, in the total  $E_{\text{DMI}}(\mathbf{q})$  these atom-related features compensate each other, resulting in a smooth  $\mathbf{q}$  dependence.

Our calculations show that the reason for the peculiar form of the partial DMI contributions is a  $\mathbf{q}$  dependent difference in the charge distribution between  $\mathbf{q}$  and  $-\mathbf{q}$  spirals. Because of total charge neutrality, these charge-distribution-related features of the atomic contributions strongly compensate each other. The physical process of the DMI formation is connected with the difference in the hybridization of the Co and Pt states under the influence of the SOC and broken spatial inversion. On the other hand, the strong  $\mathbf{q}$  dependence of the real-space distribution of the DMI energy shows that it is physically most consistent to consider the electronic hybridization as a primary effect reflecting most directly the nature of the DMI, whereas the  $\mathbf{q}$ -dependent real-space distribution of the DMI energy is a complex consequence of the processes in the electronic structure including the charge transfer process.

Also, in the dependence of the total DMI on the electron number we see clearly the traces of the compensating mechanisms. Such behavior is characteristic for the hybridized states where the lower-energy antibonding state and higher-energy bonding states give opposite contributions to the property. This behavior is in direct correlation with the statements of the importance of the anticrossing points in the band structure. The essence of the anticrossing points is the lifting of the degeneracy of the two electronic states because of a lower symmetry interaction which in the present case is the SOC.

Concerning the role of the induced Pt moments in the DMI formation, it is important that the Co-Pt hybridization leads to the spin polarization of the Pt states. This spin polarization is clearly seen in the spin-projected partial Pt DOSs. The integrated quantity, the Pt atomic spin moment, is less informative and depends on the details of the band structure of the system that are not necessarily important for the DMI. The imposed constraint of the zero Pt moment influences very weakly the spin polarization of the Pt DOS reflected in the difference of the spin-up and -down contributions to the DOS. Therefore, the hybridization mechanism leading to the different electronic energies of the  $\mathbf{q}$  and  $-\mathbf{q}$  spirals remains intact also in the case that the integrated magnetic moment vanishes.

Our ASW-qSO calculations with constraint on the Co moment have shown that also in this case there is no simple relation between the value of the Co moment and the the DMI strength. This is an additional support for the conclusion that the details of the electronic structure crucial for the DMI are not directly reflected in the integral characteristic of the atomic moments.

We briefly address the application of the ASW-qSO method to the calculation of the magnon spectrum with account for the SOC. The asymmetry of the magnon spectrum caused by the DMI and nonzero energy of the  $q = 0$  magnon due to magnetic anisotropy are correctly reproduced.

- 
- [1] A. Fert, V. Cros, and J. Sampaio, *Nat. Nanotechnol.* **8**, 152 (2013).  
 [2] S. Heinze, K. von Bergmann, M. Menzel, J. Brede, A. Kubetzka, R. Wiesendanger, G. Bihlmayer, and S. Blügel, *Nat. Phys.* **7**, 713 (2011).

- [3] N. Romming, C. Hanneken, M. Menzel, J. E. Bickel, B. Wolter, K. von Bergmann, A. Kubetzka, and R. Wiesendanger, *Science* **341**, 636 (2013).  
 [4] B. Dupe, M. Hoffmann, C. Paillard, and S. Heinze, *Nat. Commun.* **5**, 4030 (2014).

- [5] S. D. Pollard, J. A. Garlow, J. Yu, Z. Wang, Y. Zhu, and H. Yang, *Nat. Commun.* **8**, 14761 (2017).
- [6] A. Thiaville, S. Rohart, E. Jue, V. Cros, and A. Fert, *Europhys. Lett.* **100**, 57002 (2012).
- [7] I. Miron, K. Garello, G. Gaudin, P.-J. Zermatten, M. V. Costache, S. Auffret, S. Bandiera, B. Rodmacq, A. Schuhl, and P. Gambardella, *Nature (London)* **476**, 189 (2011).
- [8] K.-S. Ryu, L. Thomas, S.-H. Yang, and S. Parkin, *Nat. Nanotechnol.* **8**, 527 (2013).
- [9] N. Kanazawa, Y. Onose, T. Arima, D. Okuyama, K. Ohoyama, S. Wakimoto, K. Kakurai, S. Ishiwata, and Y. Tokura, *Phys. Rev. Lett.* **106**, 156603 (2011).
- [10] H. Katsura, N. Nagaosa, and A. V. Balatsky, *Phys. Rev. Lett.* **95**, 057205 (2005).
- [11] I. A. Sergienko and E. Dagotto, *Phys. Rev. B* **73**, 094434 (2006).
- [12] I. E. Dzyaloshinskii, *J. Phys. Chem. Solids* **4**, 241 (1958).
- [13] T. Moriya, *Phys. Rev.* **120**, 91 (1960).
- [14] Y. Ishikawa, K. Tajima, D. Bloch, and M. Roth, *Solid State Commun.* **19**, 525 (1976).
- [15] O. Nakanishi, A. Yanase, A. Hasegawa, and M. Kataoka, *Solid State Commun.* **35**, 995 (1980).
- [16] L. M. Sandratskii and J. Kübler, *Europhys. Lett.* **33**, 447 (1996).
- [17] L. M. Sandratskii, *Adv. Phys.* **47**, 91 (1998).
- [18] L. Udvardi, L. Szunyogh, K. Palotas, and P. Weinberger, *Phys. Rev. B* **68**, 104436 (2003).
- [19] I. Solovyev, N. Hamada, and K. Terakura, *Phys. Rev. Lett.* **76**, 4825 (1996).
- [20] V. V. Mazurenko and V. I. Anisimov, *Phys. Rev. B* **71**, 184434 (2005).
- [21] H. Ebert and S. Mankovsky, *Phys. Rev. B* **79**, 045209 (2009).
- [22] M. I. Katsnelson, Y. O. Kvashnin, V. V. Mazurenko, and A. I. Lichtenstein, *Phys. Rev. B* **82**, 100403(R) (2010).
- [23] M. Heide, G. Bihlmayer, and S. Blügel, *Phys. B (Amsterdam)* **404**, 2678 (2009).
- [24] Aside from the first-order perturbation approach, Ref. [23] suggests another rather cumbersome scheme for the calculation of the DMI strength. This scheme goes beyond the first-order perturbation theory and is used to show good performance of the first-order perturbation calculation.
- [25] F. Freimuth, S. Blügel, and Y. Mokrousov, *J. Phys.: Condens. Matter* **26**, 104202 (2014).
- [26] H. Yang, A. Thiaville, S. Rohart, A. Fert, and M. Chshiev, *Phys. Rev. Lett.* **115**, 267210 (2015); **118**, 219901(E) (2017).
- [27] T. Koretsune, N. Nagaosa, and R. Arita, *Sci. Rep.* **5**, 13302 (2015).
- [28] T. Kikuchi, T. Koretsune, R. Arita, and G. Tatara, *Phys. Rev. Lett.* **116**, 247201 (2016).
- [29] K.-S. Ryu, S.-H. Yang, L. Thomas, and S. S. P. Parkin, *Nat. Commun.* **5**, 3910 (2014).
- [30] L. M. Sandratskii, *Phys. Status Solidi B* **136**, 167 (1986).
- [31] B. Zimmermann, M. Heide, G. Bihlmayer, and S. Blügel, *Phys. Rev. B* **90**, 115427 (2014).
- [32] L. M. Sandratskii, *Phys. Rev. B* **64**, 134402 (2001).
- [33] M. Bode, M. Heide, K. von Bergmann, P. Ferriani, S. Heinze, G. Bihlmayer, A. Kubetzka, O. Pietzsch, S. Blügel, and R. Wiesendanger, *Nature (London)* **447**, 190 (2007).
- [34] P. Ferriani, K. von Bergmann, E. Y. Vedmedenko, S. Heinze, M. Bode, M. Heide, G. Bihlmayer, S. Blügel, and R. Wiesendanger, *Phys. Rev. Lett.* **101**, 027201 (2008).
- [35] Y. Yoshida, S. Schröder, P. Ferriani, D. Serrate, A. Kubetzka, K. von Bergmann, S. Heinze, and R. Wiesendanger, *Phys. Rev. Lett.* **108**, 087205 (2012).
- [36] S. V. Halilov, H. Eschrig, A. Y. Perlov, and P. M. Oppeneer, *Phys. Rev. B* **58**, 293 (1998).
- [37] L. M. Sandratskii, R. Singer, and E. Sasioglu, *Phys. Rev. B* **76**, 184406 (2007).
- [38] L. M. Sandratskii and G. H. Lander, *Phys. Rev. B* **63**, 134436 (2001).
- [39] L. M. Sandratskii, *Phys. Rev. B* **94**, 184414 (2016).
- [40] A. R. Williams, J. Kübler, and C. D. Gelatt, *Phys. Rev. B* **19**, 6094 (1979).
- [41] V. Eyert, *The Augmented Spherical Wave Method*, Lecture Notes in Physics (Springer, Berlin, 2012), Vol. 849.
- [42] It is worth noting that in these model calculations we neglect the hybridization between basis ASW functions assigned to the Co and Pt sites. However, each ASW is constructed in such a way that, though related to a certain atom, it contains in its tail part small contributions of the states of other atoms. Therefore, these model calculations do not remove the Co-Pt hybridization completely. However, they very clearly demonstrate the importance of the Co-Pt hybridization in the electronic states for the DMI strength.
- [43] V. Kashid, T. Schena, B. Zimmermann, Y. Mokrousov, S. Blügel, V. Shah, and H. G. Salunke, *Phys. Rev. B* **90**, 054412 (2014).
- [44] P. H. Dederichs, S. Blügel, R. Zeller, and H. Akai, *Phys. Rev. Lett.* **53**, 2512 (1984).
- [45] M. Uhl, L. M. Sandratskii, and J. Kübler, *Phys. Rev. B* **50**, 291 (1994).
- [46] L. Udvardi and L. Szunyogh, *Phys. Rev. Lett.* **102**, 207204 (2009).
- [47] K. Zakeri, Y. Zhang, J. Prokop, T.-H. Chuang, N. Sakr, W. X. Tang, and J. Kirschner, *Phys. Rev. Lett.* **104**, 137203 (2010).